

# Organic Materials

## A Nonbenzenoid 3D Nanographene Containing 5/6/7/8-Membered Rings

Pengcai Liu, Hao-Han Lv, Rui Xue, Xiao-Yu Tang, Xing-Yu Chen, Liping Qi, Xiao-Ye Wang.

Affiliations below.

DOI: 10.1055/a-2291-8774

Please cite this article as: Liu P, Lv H-H, Xue R et al. A Nonbenzenoid 3D Nanographene Containing 5/6/7/8-Membered Rings. Organic Materials 2024. doi: 10.1055/a-2291-8774

**Conflict of Interest:** The authors declare that they have no conflict of interest.

**This study was supported by** National Natural Science Foundation of China (<http://dx.doi.org/10.13039/501100001809>), 22071120, 22221002, 92256304, Fundamental Research Funds for the Central Universities (<http://dx.doi.org/10.13039/501100012226>), National Key Research and Development Program of China (<http://dx.doi.org/10.13039/501100012166>), 2020YFA0711500

### Abstract:

Nanographenes (NGs) have attracted continuous attention in recent years owing to their opened bandgaps and optoelectronic applications. Especially, nonbenzenoid NGs containing non-six-membered rings have been developed rapidly due to their unique structures and properties. In this work, we employ nonbenzenoid acepleiadylene (APD) and the cyclooctatetraene (COT) moiety to construct the first three-dimensional (3D) NG containing 5/6/7/8-membered rings in one molecule (COT-APD). The calculated results prove that COT-APD has a saddle-like configuration similar to that of other COT-type molecules. Each APD segment in COT-APD keeps the inherent aromaticity of APD moiety. Compared with other COT-type molecules, COT-APD shows a narrower bandgap, which indicates the superiority of APD in bandgap regulation. Furthermore, four reversible reductive waves are observed in electrochemical characterizations, demonstrating the excellent electron-accepting capability of COT-APD.

### Corresponding Author:

Prof. Xiao-Ye Wang, Nankai University, College of Chemistry, Weijin Road 94, 300071 Tianjin, China, [xiaoye.wang@nankai.edu.cn](mailto:xiaoye.wang@nankai.edu.cn)

### Affiliations:

Pengcai Liu, Nankai University, College of Chemistry, Tianjin, China

Hao-Han Lv, Nankai University, College of Chemistry, Tianjin, China

Rui Xue, Nankai University, College of Chemistry, Tianjin, China

[...]

Xiao-Ye Wang, Nankai University, College of Chemistry, Tianjin, China

# A Nonbenzenoid 3D Nanographene Containing 5/6/7/8-Membered Rings

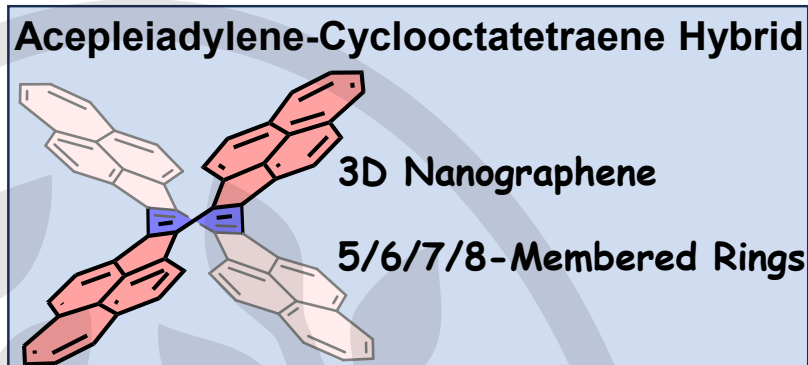
Pengcai Liu<sup>a</sup>  
 Hao-Han Lv<sup>a</sup>  
 Rui Xue<sup>a</sup>  
 Xiao-Yu Tang<sup>a</sup>  
 Xing-Yu Chen<sup>a</sup>  
 Liping Qi<sup>\*a</sup>  
 Xiao-Ye Wang<sup>\*a</sup>

<sup>a</sup> State Key Laboratory of Elemento-Organic Chemistry, Frontiers Science Center for New Organic Matter, College of Chemistry, Nankai University, Weijin Road 94, Tianjin 300071, China

\* corresponding author

E-mail: qiliping@nankai.edu.cn; xiaoye.wang@nankai.edu.cn

[Click here to insert a dedication.](#)



Received:  
 Accepted:  
 Published online:  
 DOI:

**Abstract** Nanographenes (NGs) have attracted continuous attention in recent years owing to their opened bandgaps and optoelectronic applications. Especially, nonbenzenoid NGs containing non-six-membered rings have been developed rapidly due to their unique structures and properties. In this work, we employ nonbenzenoid acepleiadylene (APD) and the cyclooctatetraene (COT) moiety to construct the first three-dimensional (3D) NG containing 5/6/7/8-membered rings in one molecule (COT-APD). The calculated results prove that COT-APD has a saddle-like configuration similar to that of other COT-type molecules. Each APD segment in COT-APD keeps the inherent aromaticity of APD moiety. Compared with other COT-type molecules, COT-APD shows a narrower bandgap, which indicates the superiority of APD in bandgap regulation. Furthermore, four reversible reductive waves are observed in electrochemical characterizations, demonstrating the excellent electron-accepting capability of COT-APD.

**Key words** Nanographene, Nonbenzenoid arene, Cyclooctatetraene, Acepleiadylene

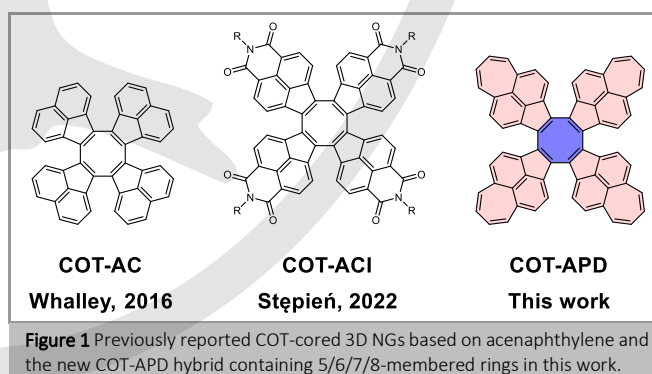
## Introduction

Nanographenes (NGs) with opened bandgaps have played a significant role in the development of next-generation semiconductors.<sup>1</sup> The bottom-up chemical syntheses of NGs have not only provided atomically precise structures,<sup>2</sup> but also enabled the creation of NGs with novel topologies.<sup>3</sup> For example, nonbenzenoid NGs with non-six-membered rings have been extensively developed<sup>4</sup> in recent years, showing intriguing properties and applications.<sup>5</sup> However, the reported ring topologies have still been limited. An intriguing type of nonbenzenoid NGs with multiple different rings (e.g. 5/6/7/8-membered rings) merged in a single molecule has remained elusive.

Acepleiadylene (APD) is a nonbenzenoid arene containing 5/6/7-membered rings, and has been employed as a unique building block for NGs and optoelectronic materials.<sup>6</sup> On the other hand, cyclooctatetraene (COT), an 8 $\pi$  nonaromatic ring, has often been

used for the construction of 3D saddle-shaped conjugated molecules.<sup>7</sup> Nevertheless, only very few examples of COT-based NGs have been reported, such as the acenaphthylene-fused COT (COT-AC) by Whalley et al. and its imide-functionalized derivatives (COT-ACI) by Stępień et al. (Figure 1), as well as the hexa-*peri*-hexabenzocoronene-fused COT by Martín et al.<sup>8</sup> Thus, COT-based 3D NGs, especially nonbenzenoid NGs, have been largely underexplored.

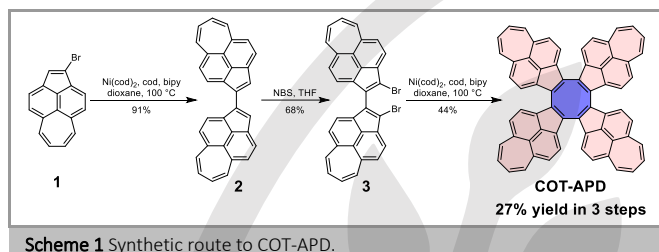
Herein, we report the synthesis and characterizations of a new COT-APD hybrid as a Nonbenzenoid 3D NG, which represents the first NG bearing 5/6/7/8-membered rings in the same backbone (Figure 1). Compared with COT-AC, COT-APD has a larger  $\pi$  system and a narrower bandgap. Furthermore, as a pure hydrocarbon molecule, COT-APD exhibits four reversible reductive waves in cyclic voltammetry (CV) characterizations, indicating its strong electron-accepting capability.



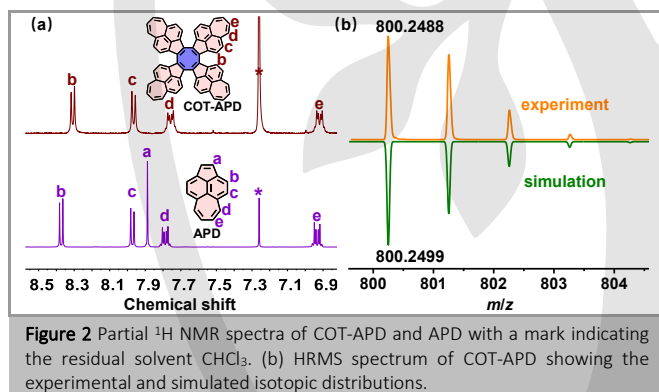
## Results and Discussion

The synthetic route to COT-APD is shown in Scheme 1. A Yamamoto coupling of monobrominated APD **1** gave APD dimer **2** in 91% yield, which was subsequently brominated on the two five-membered rings to afford compound **3** in 68% yield. Another

Yamamoto coupling of two brominated APD dimer achieved the target molecule in 44% yield.<sup>9</sup> The three-step route realized the synthesis of the nonbenzenoid 3D NG in a 27% overall yield. All compounds were characterized by nuclear magnetic resonance (NMR) and high-resolution mass spectrometry (HRMS) to verify their chemical structures. The solubility of COT-APD in common organic solvents is relatively low (e.g., 0.26 mg mL<sup>-1</sup> in toluene), which hampered the growth of single crystals for X-ray analysis.

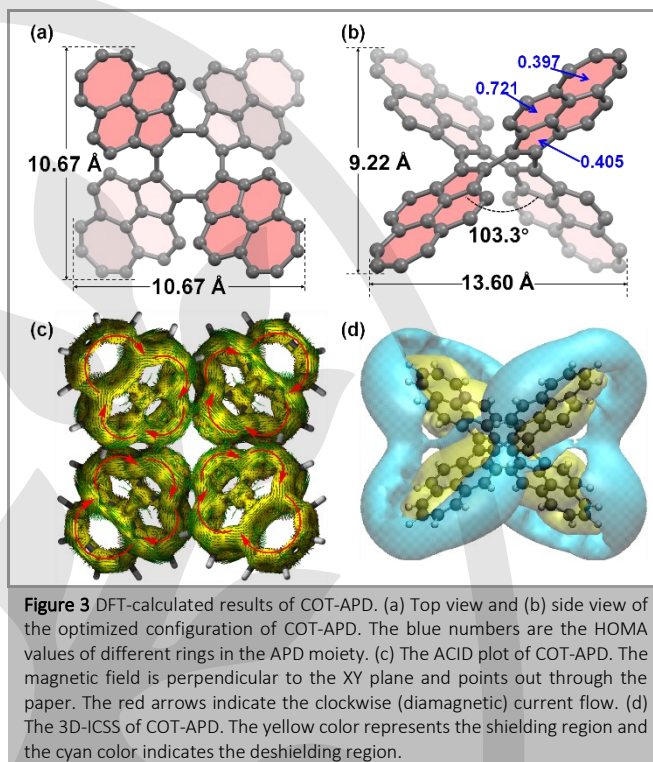


As shown in Figure 2a, COT-APD exhibits similar <sup>1</sup>H NMR chemical shifts compared with its monomer APD, which implies that the chemical environment of each APD moiety in COT-APD is similar to that of the monomer. The slight upfield shift of all proton signals in COT-APD results from the stronger electron-donating effect of the sp<sup>2</sup> carbon in the COT ring than hydrogen in APD. The HRMS spectrum of COT-APD shows a molecular ion signal at *m/z* = 800.2488 Da, in good agreement with the expected molecular mass of 800.2499 Da for C<sub>64</sub>H<sub>32</sub> with the relative error of 1.4 ppm. The experimental isotopic distribution also matches well with the simulated pattern, clearly proving the chemical identity of COT-APD (Figure 2b).



In order to further understand the configuration and properties of COT-APD, density functional theory (DFT) calculations in the gas phase were performed (Figure 3). The optimized geometry suggests that the molecular size of COT-APD is in nanoscale. Furthermore, COT-APD distorts apparently with a dihedral angle of 103.3° between the two opposite APD moieties. It shows a saddle-like configuration, and belongs to *D*<sub>2d</sub> point group. The harmonic oscillator model of aromaticity (HOMA) values<sup>10</sup> were calculated according to the optimized structure. The positive values (Figure 3b) of the rings in the APD moiety proves that the aromaticity of APD is kept in COT-APD. The anisotropy of the induced current density (ACID) plot<sup>11</sup> (Figure 3c) of COT-APD suggests that each APD segment maintains the intrinsic aromaticity of its monomer with the clockwise ring current flow in each segment, while the central COT ring does not display continuous ring current flow, exhibiting nonaromaticity which is

a typical feature for COT. The 3D iso-chemical shift shielding surface (ICSS)<sup>12</sup> indicates that the space above and below each APD segment is the shielding region (yellow isosurface), while the space around each APD segment is the deshielding region (blue isosurface).



In order to study the photophysical properties, the UV-Vis absorption spectrum of COT-APD in a toluene solution was recorded (Figure 4a). The absorption spectrum of COT-APD features an absorption maximum at 386 nm with additional fine structures at 474, 554, and 604 nm. The absorption onset of COT-APD (639 nm) is red-shifted compared with that of its monomer APD (565 nm), indicating a narrower optical gap upon COT fusion (APD: 2.19 eV; COT-APD: 1.94 eV). Compared with other COT-based molecules, COT-APD also exhibits an apparently narrower optical gap (Table S1). The fluorescence spectrum shows an emission maximum at 787 nm in the near-infrared region (Figure S2).

To shed light on the absorption feature of COT-APD, time-dependent (TD) DFT calculations were carried out. The simulated spectrum resembles well the experimental result (Figure 4b). The transition from *S*<sub>0</sub> to *S*<sub>1</sub> is forbidden with an oscillator strength of 0. The *S*<sub>0</sub>→*S*<sub>2</sub> and *S*<sub>0</sub>→*S*<sub>3</sub> excitations are equal in energy and are mainly contributed by the transitions from degenerate HOMO-1 and HOMO-2 to LUMO, respectively (Table S2). Similarly, the *S*<sub>0</sub>→*S*<sub>6</sub> and *S*<sub>0</sub>→*S*<sub>7</sub> excitations are mainly contributed by the transitions from HOMO to degenerate LUMO+1 and LUMO+2, respectively. The degenerate orbitals of COT-APD stem from its high symmetry. Note that the HOMO is mainly localized on the COT moiety, while the LUMO is distributed over the whole backbone (Figure 4c). Therefore, the COT ring has a significant contribution to the absorption feature of COT-APD.

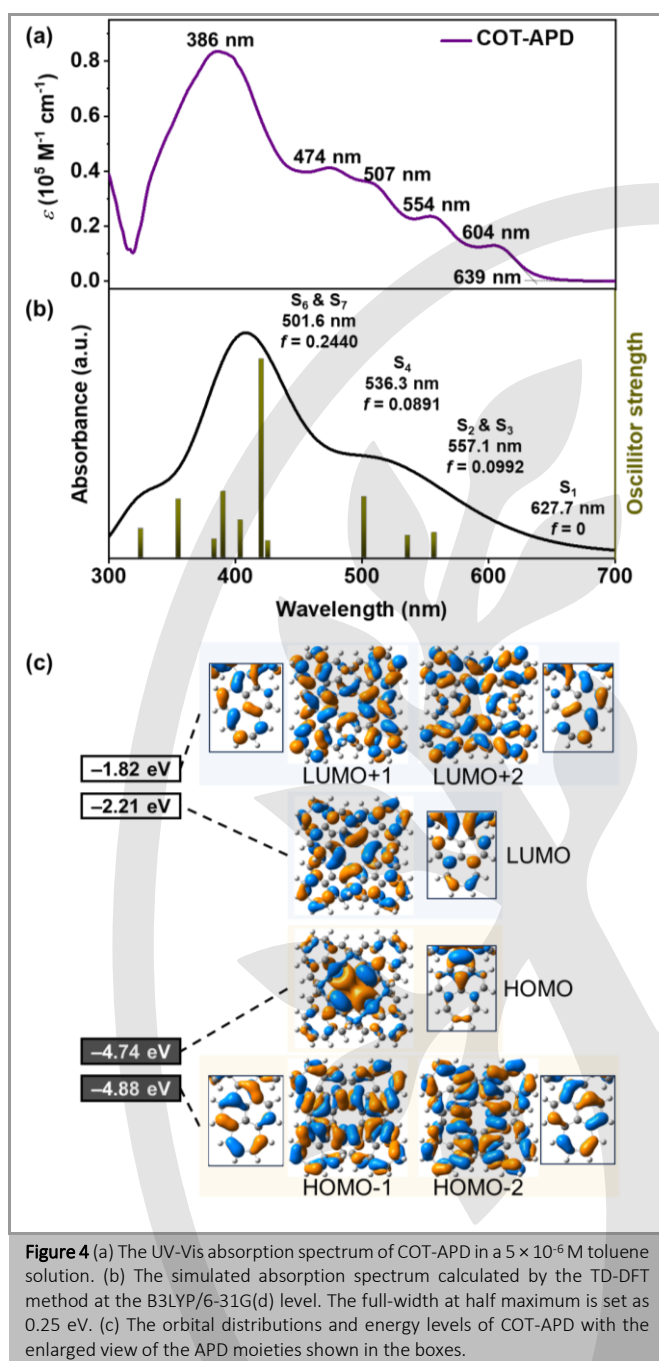


**Figure 4** (a) The UV-Vis absorption spectrum of COT-APD in a  $5 \times 10^{-6}$  M toluene solution. (b) The simulated absorption spectrum calculated by the TD-DFT method at the B3LYP/6-31G(d) level. The full-width at half maximum is set as 0.25 eV. (c) The orbital distributions and energy levels of COT-APD with the enlarged view of the APD moieties shown in the boxes.

To characterize the redox properties of COT-APD, cyclic voltammetry (CV) and differential pulse voltammetry (DPV) measurements were conducted (Figure 5a). COT-APD exhibits an irreversible oxidation wave with an onset at 0.47 V, which is lower than that of APD (0.58 V) (Figure S3). Interestingly, the 3D NG shows four reversible reductive waves with the half-wave potentials at -1.65 V, -1.84 V, -2.38 V, and -2.56 V, demonstrating the excellent electron-accepting capability of COT-APD, which may come from the electron-accepting capability of APD as revealed by Müllen et al. in 1980.<sup>13</sup> Four reductive peaks are also observed in DPV measurement, in accordance with the CV result. Because the oxidation is irreversible, the HOMO and LUMO energy levels of COT-APD are determined by the onsets of oxidative and reductive waves, respectively, with ferrocene as an external standard. COT-APD exhibits a higher HOMO level and a lower LUMO level than the monomer APD, indicating the

extended  $\pi$ -conjugation in the tetramer (Figure 5b). Compared with COT-AC, COT-APD shows a similar LUMO energy level (-3.22 eV for COT-APD, -3.26 eV for COT-AC), but a higher HOMO energy level (-5.25 eV for COT-APD, -5.37 eV for COT-AC). As a result, COT-APD displays a narrower HOMO-LUMO gap than COT-AC, which is consistent with the optical gap results.

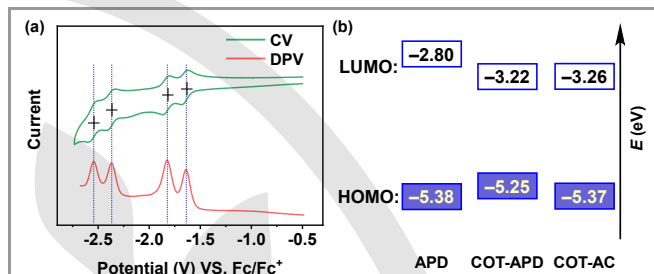


**Figure 5** (a) The electrochemical reduction properties of COT-APD. (b) The electrochemical energy gap of APD, COT-APD, and COT-AC.

## Conclusions

In summary, the synthesis of the first NG containing 5/6/7/8-membered rings in the same backbone has been achieved by fusing the APD and COT moieties. Theoretical calculations reveal that COT-APD displays a saddle-shaped configuration. The absorption spectrum illustrates the narrow optical bandgap of COT-APD, which is in accordance with the electrochemical HOMO-LUMO gap. Furthermore, four reversible reductive waves of COT-APD demonstrate its strong electron-accepting capability, significantly different from the previously reported COT-based NGs. This work not only provides a novel nonbenzenoid NG with 3D configuration, but also demonstrates the high potential of the novel COT-APD hybrid as functional materials.

## Funding Information

This work was financially supported by the National Natural Science Foundation of China (22071120, 92256304, 22221002), the National Key R&D Program of China (2020YFA0711500), and the Fundamental Research Funds for the Central Universities.

## Acknowledgment

The authors extend their gratitude to Ms. Shudi Ren from Shiyanjia Lab ([www.shiyanjia.com](http://www.shiyanjia.com)) for providing invaluable assistance with the HRMS tests.

## Supporting Information

YES (this text will be updated with links prior to publication)

## Primary Data

NO.

## Conflict of Interest

The authors declare no conflict of interest.

## References and Notes

- (1) (a) Narita, A.; Wang, X.-Y.; Feng, X.; Müllen, K. *Chem. Soc. Rev.* **2015**, *44*, 6616. (b) Wang, X.-Y.; Yao, X.; Müllen, K. *Sci. China Chem.* **2019**, *62*, 1099.
- (2) (a) Zhu, Y.; Wang, J. *Acc. Chem. Res.* **2023**, *56*, 363. (b) Senese, A.; Chalifoux, W. *Molecules* **2018**, *24*, 118.
- (3) (a) Anderson, H. V.; Gois, N. D.; Chalifoux, W. A. *Org. Chem. Front.* **2023**, *10*, 4167. (b) Hermann, M.; Wassy, D.; Esser, B. *Angew. Chem. Int. Ed.* **2021**, *60*, 15743.
- (4) (a) Chaolumen; Stepek, I. A.; Yamada, K. E.; Ito, H.; Itami, K. *Angew. Chem. Int. Ed.* **2021**, *60*, 23508. (b) Pun, S. H.; Miao, Q. *Acc. Chem. Res.* **2018**, *51*, 1630. (c) Xin, H.; Hou, B.; Gao, X. *Acc. Chem. Res.* **2021**, *54*, 1737. (d) Konishi, A.; Yasuda, M. *Chem. Lett.* **2021**, *50*, 195. (e) Shimizu, A.; Morikoshi, T.; Sugisaki, K.; Shiomi, D.; Sato, K.; Takui, T.; Shintani, R. *Angew. Chem. Int. Ed.* **2022**, *61*, e202205729. (f) Horii, K.; Kishi, R.; Nakano, M.; Shiomi, D.; Sato, K.; Takui, T.; Konishi, A.; Yasuda, M. *J. Am. Chem. Soc.* **2022**, *144*, 3370. (g) Wang, Y.; Huang, Y.; Huang, T.; Zhang, J.; Luo, T.; Ni, Y.; Li, B.; Xie, S.; Zeng, Z. *Angew. Chem. Int. Ed.* **2022**, *61*, e202200855. (h) Ma, J.; Fu, Y.; Dmitrieva, E.; Liu, F.; Komber, H.; Hennersdorf, F.; Popov, A. A.; Weigand, J. J.; Liu, J.; Feng, X. *Angew. Chem. Int. Ed.* **2020**, *59*, 5637. (i) Fei, Y.; Fu, Y.; Bai, X.; Du, L.; Li, Z.; Komber, H.; Low, K.-H.; Zhou, S.; Phillips, D. L.; Feng, X.; Liu, J. *J. Am. Chem. Soc.* **2021**, *143*, 2353. (j) Mallada, B.; de la Torre, B.; Mendieta-Moreno, J. I.; Nachtigallová, D.; Matěj, A.; Matoušek, M.; Mutombo, P.; Brabec, J.; Veis, L.; Cadart, T.; Kitora, M.; Jelínek, P. *J. Am. Chem. Soc.* **2021**, *143*, 14694. (k) Park, S.; Kim, C.-E.; Jeong, J.; Ryu, H.; Maeng, C.; Kim, D.; Baik, M.-H.; Lee, P. H. *Nat. Commun.* **2023**, *14*, 7936. (l) Liu, B.; Chen, M.; Liu, X.; Fu, R.; Zhao, Y.; Duan, Y.; Zhang, L. *J. Am. Chem. Soc.* **2023**, *145*, 28137. (m) Yamada, K. E.; Stepek, I. A.; Matsuoka, W.; Ito, H.; Itami, K. *Angew. Chem. Int. Ed.* **2023**, *62*, e202311770. (n) Sanil, G.; Krzeszewski, M.; Chaładaj, W.; Danikiewicz, W.; Knysh, I.; Dobrzycki, Ł.; Staszewska-Krajewska, O.; Cyrański, M. K.; Jacquemin, D.; Gryko, D. T. *Angew. Chem. Int. Ed.* **2023**, *62*, e202311123. (o) Luo, H.; Liu, J. *Angew. Chem. Int. Ed.* **2023**, *62*, e202302761. (p) Borstelmann, J.; Bergner, J.; Rominger, F.; Kivala, M. *Angew. Chem. Int. Ed.* **2023**, *62*, e202312740. (q) Liu, R.; Fu, Y.; Wu, F.; Liu, F.; Zhang, J. J.; Yang, L.; Popov, A. A.; Ma, J.; Feng, X. *Angew. Chem. Int. Ed.* **2023**, *62*, e202219091. (r) Segawa, Y. *Chem* **2023**, *9*, 2725.
- (5) (a) Zhang, X. S.; Huang, Y. Y.; Zhang, J.; Meng, W.; Peng, Q.; Kong, R.; Xiao, Z.; Liu, J.; Huang, M.; Yi, Y.; Chen, L.; Fan, Q.; Lin, G.; Liu, Z.; Zhang, G.; Jiang, L.; Zhang, D. *Angew. Chem. Int. Ed.* **2020**, *59*, 3529. (b) Ikai, T.; Oki, K.; Yamakawa, S.; Yashima, E. *Angew. Chem. Int. Ed.* **2023**, *62*, e202301836. (c) Yang, L.; Ju, Y. Y.; Medel, M. A.; Fu, Y.; Komber, H.; Dmitrieva, E.; Zhang, J. J.; Obermann, S.; Campaña, A. G.; Ma, J.; Feng, X. *Angew. Chem. Int. Ed.* **2023**, *62*, e202216193. (d) Qiu, Z. L.; Chen, X. W.; Huang, Y. D.; Wei, R. J.; Chu, K. S.; Zhao, X. J.; Tan, Y. Z. *Angew. Chem. Int. Ed.* **2022**, *61*, e202116955. (e) Qin, L.; Huang, Y. Y.; Wu, B.; Pan, J.; Yang, J.; Zhang, J.; Han, G.; Yang, S.; Chen, L.; Yin, Z.; Shu, Y.; Jiang, L.; Yi, Y.; Peng, Q.; Zhou, X.; Li, C.; Zhang, G.; Zhang, X. S.; Wu, K.; Zhang, D. *Angew. Chem. Int. Ed.* **2023**, *62*, e202304632. (f) Xin, H.; Ge, C.; Jiao, X.; Yang, X.; Rundel, K.; McNeill, C. R.; Gao, X. *Angew. Chem. Int. Ed.* **2017**, *57*, 1322. (g) Yang, X.; Rominger, F.; Mastalerz, M. *Angew. Chem. Int. Ed.* **2019**, *58*, 17577. (h) Xin, H.; Li, J.; Lu, R.-Q.; Gao, X.; Swager, T. M. *J. Am. Chem. Soc.* **2020**, *142*, 13598. (i) Ogawa, N.; Yamaoka, Y.; Takikawa, H.; Yamada, K.-i.; Takasu, K. *J. Am. Chem. Soc.* **2020**, *142*, 13322. (j) Lu, X.; Gopalakrishna, T. Y.; Han, Y.; Ni, Y.; Zou, Y.; Wu, J. *J. Am. Chem. Soc.* **2019**, *141*, 5934. (k) Zou, Y.; Zeng, W.; Gopalakrishna, T. Y.; Han, Y.; Jiang, Q.; Wu, J. *J. Am. Chem. Soc.* **2019**, *141*, 7266.
- (6) (a) Liu, P.; Chen, X.-Y.; Cao, J.; Ruppenthal, L.; Gottfried, J. M.; Müllen, K.; Wang, X.-Y. *J. Am. Chem. Soc.* **2021**, *143*, 5314. (b) Fu, L.; Liu, P.; Xue, R.; Tang, X. Y.; Cao, J.; Yao, Z. F.; Liu, Y.; Yan, S.; Wang, X. Y. *Angew. Chem. Int. Ed.* **2023**, *62*, e202306509. (c) Liu, P.; Fu, L.; Tang, X.-Y.; Xue, R.; Zhang, L.; Cao, J.; Wang, X.-Y. *J. Mater. Chem. C* **2023**, *11*, 10149. (d) Liu, P.; Tang, X.-Y.; Du, C.-Z.; Xue, R.; Chen, X.-Y.; Cao, J.; Wang, X.-Y. *Sci. China Chem.* **2023**, *66*, 3506.
- (7) (a) Marsella, M. J. *Acc. Chem. Res.* **2002**, *35*, 944. (b) Wang, C.; Xi, Z. *Chem. Commun.* **2007**, 5119. (c) Yamakado, T.; Saito, S. *J. Am. Chem. Soc.* **2022**, *144*, 2804. (d) Kotani, R.; Yokoyama, S.; Nobusue, S.; Yamaguchi, S.; Osuka, A.; Yabu, H.; Saito, S. *Nat. Commun.* **2022**, *13*, 303. (e) Suga, K.; Yamakado, T.; Saito, S. *J. Am. Chem. Soc.* **2023**, *145*, 26799.
- (8) (a) Urieta-Mora, J.; Krug, M.; Alex, W.; Perles, J.; Fernández, I.; Molina-Ontoria, A.; Guldi, D. M.; Martín, N. *J. Am. Chem. Soc.* **2020**, *142*, 4162. (b) Kumar, R.; Chmielewski, P. J.; Lis, T.; Volkmer, D.; Stępień, M. *Angew. Chem. Int. Ed.* **2022**, *61*, e202207486. (c) Sumy, D. P.; Dodge, N. J.; Harrison, C. M.; Finke, A. D.; Whalley, A. C. *Chem. Eur. J.* **2016**, *22*, 4709.
- (9) Cyclooctatetraacepleiadylene (COT-APD) was prepared by the Yamamoto coupling of compound **3**. A typical procedure for the synthesis of COT-APD is described as follows. To a Schlenk flask charged with compound **3** (50.4 mg, 0.0900 mmol), Ni(cod)<sub>2</sub> (49.5 mg, 0.180 mmol), 1,5-cyclooctadiene (19.5 mg, 0.180 mmol) and 2,2'-bipyridine (28.1 mg, 0.180 mmol) was added dioxane (4.5 mL) under argon. Then the mixture was heated to 100 °C for 16 h. After cooling to room temperature, the mixture was filtrated and the residue was sequentially washed by MeOH, HCl (2 M), EtOH, and CH<sub>2</sub>Cl<sub>2</sub>. The obtained solid was dried in vacuo to afford 15.9 mg (yield: 44%) of COT-APD as a black solid. <sup>1</sup>H NMR (400 MHz, CS<sub>2</sub>/CDCl<sub>3</sub>, 297 K, ppm) δ 8.300 (d, J = 7.5 Hz, 8H), 7.961 (d, J = 7.6 Hz, 8H), 7.793 – 7.710 (m, 8H), 6.958 – 6.881 (m, 8H). <sup>13</sup>C NMR (101 MHz, CS<sub>2</sub>/CDCl<sub>3</sub>, 297 K, ppm) δ 137.98, 136.96, 135.49, 127.54, 127.06, 126.68. HRMS (MALDI) m/z: Calcd. for C<sub>64</sub>H<sub>32</sub><sup>+</sup>, 800.2499; Found: 800.2488 [M]<sup>+</sup>.
- (10) Krygowski, T. M.; Cyrański, M. K. *Phys. Chem. Chem. Phys.* **2004**, *6*, 249.
- (11) Geuenich, D.; Hess, K.; Köhler, F.; Herges, R. *Chem. Rev.* **2005**, *105*, 3758.
- (12) (a) Klod, S.; Kleinpeter, E. *J. Chem. Soc., Perkin Trans. 2* **2001**, 1893. (b) Lu, T.; Chen, F. *J. Comput. Chem.* **2011**, *33*, 580.
- (13) Becker, B. C.; Huber, W.; Müllen, K. *J. Am. Chem. Soc.* **1980**, *102*, 7805.

# Supporting Information

for

## A Nonbenzenoid 3D Nanographene Containing 5/6/7/8-Membered Rings

Pengcai Liu<sup>a</sup>, Hao-Han Lv<sup>a</sup>, Rui Xue<sup>a</sup>, Xiao-Yu Tang<sup>a</sup>, Xing-Yu Chen<sup>a</sup>, Liping Qi<sup>\*,a</sup>  
Xiao-Ye Wang<sup>\*,a</sup>

<sup>a</sup> State Key Laboratory of Element-Organic Chemistry, Frontiers Science Center for New Organic Matter,  
College of Chemistry, Nankai University, Weijin Road 94, Tianjin 300071, China

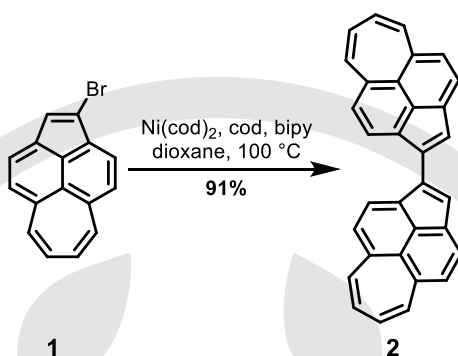
### Table of contents

1. General methods .....	2
2. Synthetic procedure .....	3
3. Photophysical and electrochemical properties.....	5
4. Theoretical calculations .....	7
5. References.....	12
6. NMR spectra .....	13

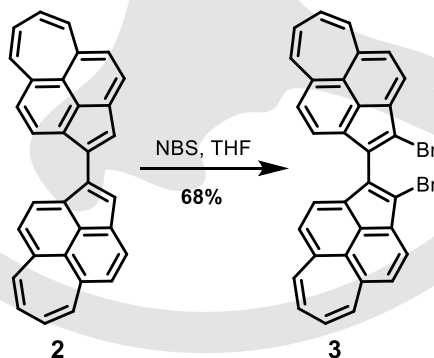
## 1. General methods

All commercial reagents and solvents were used as received without further purification unless otherwise mentioned. Anhydrous  $\text{CH}_2\text{Cl}_2$ , toluene and tetrahydrofuran (THF) were obtained from an Ultimate Solvent System 4S (USS-4S). Column chromatography was performed with silica gel (particle size 0.063-0.200 mm) and thin layer chromatography (TLC) was performed on silica gel with GF254 indicator. All yields given referred to isolated yields unless otherwise noted. Nuclear magnetic resonance (NMR) spectra were recorded on an AVANCE 400 MHz Bruker spectrometer. Chemical shifts were reported in ppm. Coupling constants ( $J$  values) were reported in Hertz.  $^1\text{H}$  NMR chemical shifts were referenced to  $\text{CHCl}_3$  (7.260 ppm).  $^{13}\text{C}$  NMR chemical shifts were referenced to  $\text{CDCl}_3$  (77.00 ppm). The following abbreviations were used for multiplicities: s = singlet, d = doublet, m = multiplet. High-resolution mass spectrometry (HRMS) was performed on a VG ZAB-HS MRMS by matrix assisted laser desorption ionization (MALDI). UV-Vis absorption spectra were recorded on an Analytikjena Specord 210 Plus UV-Vis spectrophotometer. Steady-state fluorescence spectra were recorded on an Edinburgh FS5 Spectrofluorometer. The electrochemical measurements were carried out in anhydrous THF containing 0.1 M  $n\text{-Bu}_4\text{NPF}_6$  as supporting electrolyte (scan rate:  $100 \text{ mV s}^{-1}$ .) under an argon atmosphere on a CHI 620E electrochemical analyzer. A three-electrode system with glassy carbon as working electrode,  $\text{Ag}/\text{AgCl}$  as reference electrode, platinum wire as counter electrode was applied. The potential was calibrated against ferrocene/ferrocenium couple.

## 2. Synthetic procedure



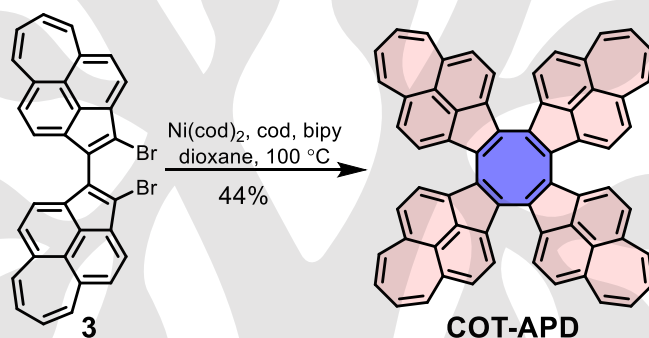
**1,1'-bi(cyclohepta[fg]acenaphthylene) (2).** To a Schlenk flask charged with compound **1**<sup>1</sup> (50.0 mg, 0.179 mmol),  $\text{Ni}(\text{cod})_2$  (98.5 mg, 0.358 mmol), 2,2'-bipyridine (55.9 mg, 0.358 mmol), and 1,5-cyclooctadiene (38.7 mg, 0.358 mmol) was added dioxane (2 mL) under argon. Then the mixture was heated to  $100\text{ }^\circ\text{C}$  for 16 h. After cooling to room temperature, the mixture was filtrated under vacuum and washed by  $\text{CH}_2\text{Cl}_2$ , and then the filtrate was collected. After removal of the solvent under reduced pressure, the residue was purified by flash column chromatography over silica gel (eluent: hexane/ $\text{CH}_2\text{Cl}_2 = 3 : 1$ ) to afford 32.6 mg (yield: 91%) of **2** as a dark red solid.  $^1\text{H}$  NMR (400 MHz,  $\text{CDCl}_3$ , 297 K, ppm)  $\delta$  8.839 (d,  $J = 7.4$  Hz, 2H), 8.420 (d,  $J = 7.3$  Hz, 2H), 8.352 (s, 2H), 8.056 (d,  $J = 7.5$  Hz, 2H), 7.992 (d,  $J = 7.4$  Hz, 2H), 7.786 (d,  $J = 11.0$  Hz, 4H), 6.995 – 6.879 (m, 4H).  $^{13}\text{C}$  NMR (101 MHz,  $\text{CS}_2/\text{CDCl}_3$ , 297 K, ppm)  $\delta$  138.43, 137.74, 137.33, 136.65, 135.33, 134.73, 133.83, 127.77, 127.70, 127.50, 127.39, 126.66, 126.19, 125.26, 124.32. HRMS (MALDI)  $m/z$ : Calcd. for  $\text{C}_{32}\text{H}_{18}^+$ , 402.1403; Found: 402.1402  $[\text{M}]^+$ .



**2,2'-dibromo-1,1'-bi(cyclohepta[fg]acenaphthylene) (3).** To a flask charged with compound **2** (32.6 mg, 0.0810 mmol) was added THF (8 mL). Then N-



bromosuccinimide (31.7 mg, 0.178 mmol) was added portionwise. The mixture was stirred at 25 °C for 12 h. After quenching with H<sub>2</sub>O, the reaction mixture was extracted with CH<sub>2</sub>Cl<sub>2</sub> for three times. The combined organic layers were washed with water and brine and dried over MgSO<sub>4</sub>. After removal of the solvent under reduced pressure, the residue was purified by column chromatography over silica gel (eluent: hexane/ CH<sub>2</sub>Cl<sub>2</sub> = 3 : 1) and recrystallization from CH<sub>2</sub>Cl<sub>2</sub>/MeOH to give 31.0 mg (yield: 68%) of **3** as a black solid. <sup>1</sup>H NMR (400 MHz, CDCl<sub>3</sub>, 297 K, ppm) δ 8.512 (d, *J* = 7.5 Hz, 2H), 8.241 (d, *J* = 7.5 Hz, 2H), 8.107 (d, *J* = 7.6 Hz, 2H), 7.954 (d, *J* = 7.6 Hz, 2H), 7.915 – 7.857 (m, 2H), 7.853 – 7.787 (m, 2H), 7.099 – 6.980 (m, 4H). The <sup>13</sup>C NMR spectrum could not be obtained even with the number of scans over 10000 due to the poor solubility of **3**. HRMS (MALDI) *m/z*: Calcd. for C<sub>32</sub>H<sub>16</sub>Br<sub>2</sub><sup>+</sup>, 557.9613; Found: 557.9612 [M]<sup>+</sup>.



**Cyclooctatetraacepleiadylene (COT-APD).** To a Schlenk flask charged with compound **3** (50.4 mg, 0.0900 mmol), Ni(cod)<sub>2</sub> (49.5 mg, 0.180 mmol), 1,5-cyclooctadiene (19.5 mg, 0.180 mmol) and 2,2'-bipyridine (28.1 mg, 0.180 mmol) was added dioxane (4.5 mL) under argon. Then the mixture was heated to 100 °C for 16 h. After cooling to room temperature, the mixture was filtrated and the residue was sequentially washed by MeOH, HCl (2M), EtOH, and CH<sub>2</sub>Cl<sub>2</sub>. The obtained solid was dried in vacuo to afford 15.9 mg (yield: 44%) of **COT-APD** as a black solid. <sup>1</sup>H NMR (400 MHz, CS<sub>2</sub>/CDCl<sub>3</sub>, 297 K, ppm) δ 8.300 (d, *J* = 7.5 Hz, 8H), 7.961 (d, *J* = 7.6 Hz, 8H), 7.793 – 7.710 (m, 8H), 6.958 – 6.881 (m, 8H). <sup>13</sup>C NMR (101 MHz, CS<sub>2</sub>/CDCl<sub>3</sub>, 297 K, ppm) δ 137.98, 136.96, 135.49, 127.54, 127.06, 126.68. HRMS (MALDI) *m/z*: Calcd. for C<sub>64</sub>H<sub>32</sub><sup>+</sup>, 800.2499; Found: 800.2488 [M]<sup>+</sup>.

### 3. Photophysical and electrochemical properties

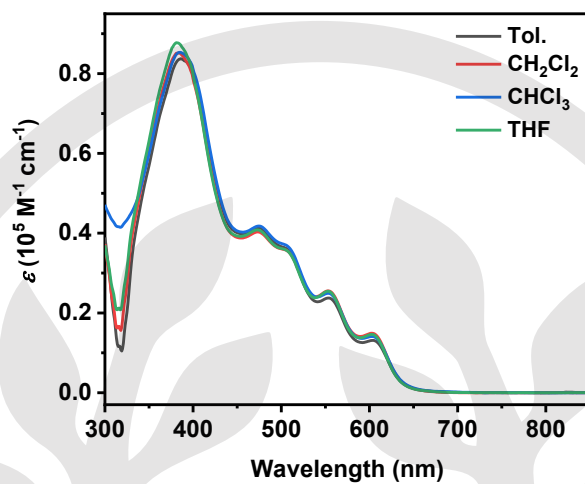


**Figure S1.** The absorption spectra of COT-APD in toluene,  $\text{CH}_2\text{Cl}_2$ ,  $\text{CHCl}_3$ , and THF solutions ( $5 \times 10^{-6}$  M).

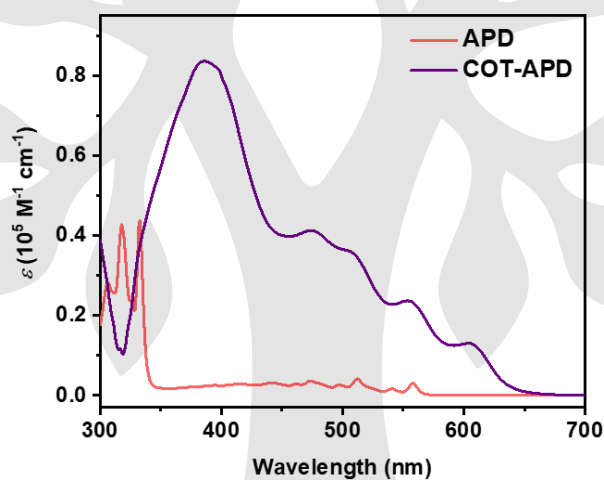


**Figure S2.** The absorption spectra of APD and COT-APD in toluene solutions ( $5 \times 10^{-6}$  M).

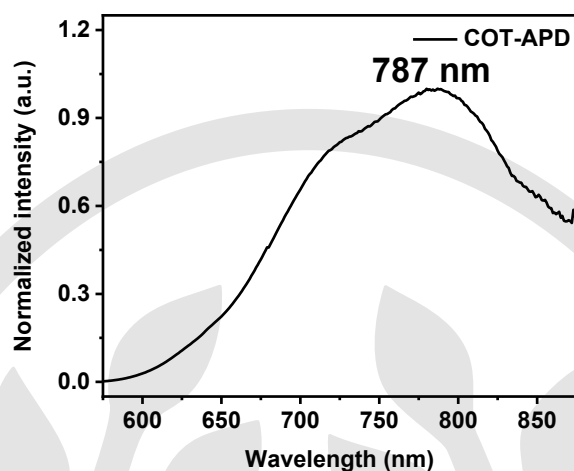


**Figure S3.** The fluorescence spectrum of COT-APD in toluene solution ( $5 \times 10^{-6}$  M) with the excitation wavelength of 385 nm.

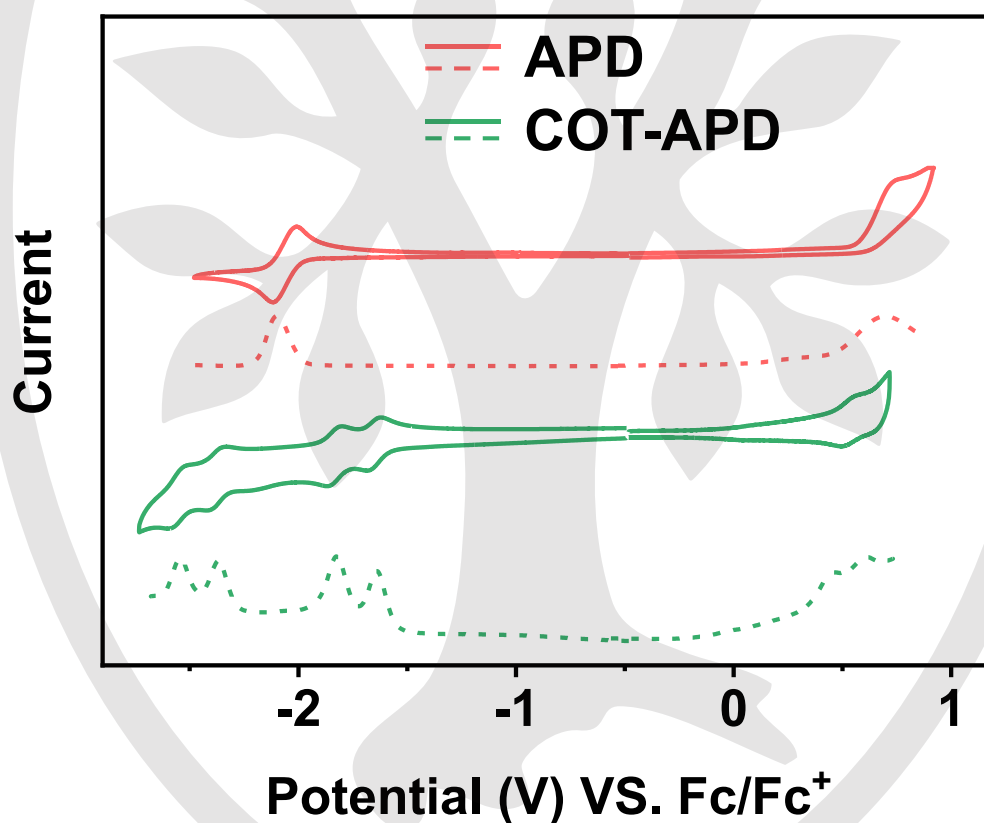


**Figure S4.** Cyclic voltammograms (CV) and differential pulse voltammograms (DPV) of APD and COT-APD in THF with 0.1 M *n*-Bu<sub>4</sub>NPF<sub>6</sub> as supporting electrolyte and ferrocene as an external standard.

**Table S1.** Comparison of the properties of APD, COT-APD, and other reported COT-type molecules.<sup>a</sup>

Compound	$\lambda_{\text{onset}}$ (nm)	$E_{\text{g}}^{\text{opt}}$ (eV)	LUMO <sup>CV</sup> (eV)	HOMO <sup>CV</sup> (eV)	$E_{\text{g}}^{\text{CV}}$ (eV)	Ref.
APD	565	2.19	-2.80	-5.38	2.58	2
COT-APD	639	1.94	-3.22	-5.25	2.03	this work
COT-AC	~530 <sup>b</sup>	2.34	-3.26	-5.37	2.11	3
COT-ACI	~600 <sup>b</sup>	2.07	-3.92	-5.81	1.89	4
COT-HBC	~460 <sup>b</sup>	2.70	--	-5.72	--	5

Definition: <sup>a</sup>The  $\lambda_{\text{onset}}$  refers to the lowest energy absorption onset in the absorption spectra. The  $E_{\text{g}}^{\text{opt}}$  is the optical energy gap calculated by the equation  $E_{\text{g}}^{\text{opt}} = 1240/\lambda_{\text{onset}}$ . The LUMO<sup>CV</sup> and HOMO<sup>CV</sup> energy levels are calculated based on the onset potentials of the first reductive and oxidative waves, respectively. <sup>b</sup>The  $\lambda_{\text{onset}}$  is estimated according to the absorption spectra in the corresponding literature.

#### 4. Theoretical calculations

Theoretical calculations were performed using the Gaussian 09 software package.<sup>6</sup> All calculations were carried out using the density functional theory (DFT) or time-dependent DFT (TD-DFT) method in the gas phase. The geometries were optimized using DFT method at the B3LYP/6-31G(d) level. TD-DFT calculation based on the S<sub>0</sub> geometry was performed at the B3LYP/6-31G(d) level. Anisotropy of the induced current density (ACID) plot was calculated by using the method developed by Herges.<sup>7</sup> Nucleus-independent chemical shifts (NICS)<sup>8</sup> calculations were performed at the B3LYP/6-311++G(2d,p) level. The isochemical shielding surface (ICSS) and the harmonic oscillator model of aromaticity (HOMA)<sup>9</sup> calculations were carried out by using Multiwfn.<sup>10</sup> Electron density of delocalized bond (EDDB)<sup>11</sup> calculations were carried out at the B3LYP/6-31G(d) level.

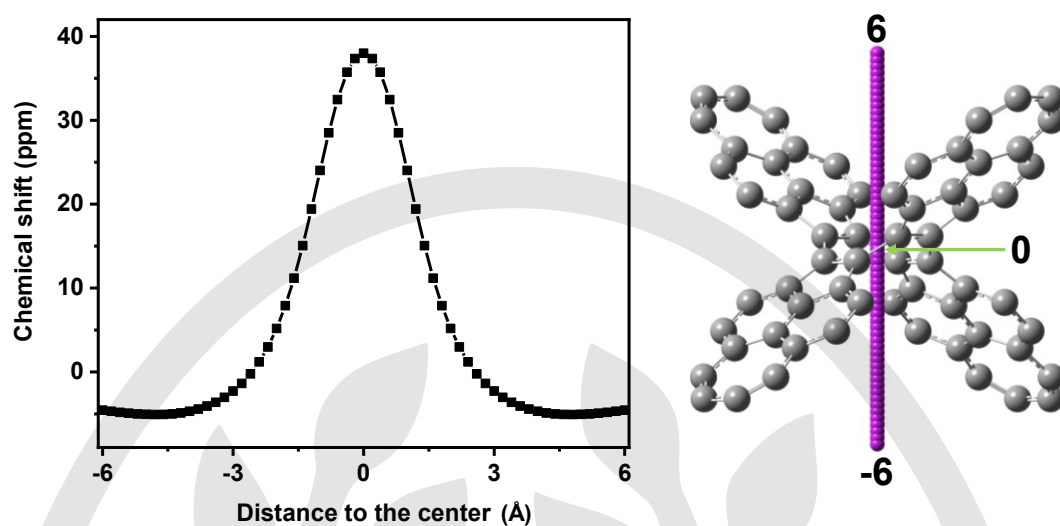


**Figure S5.** NICS scan along the direction perpendicular to the COT ring.

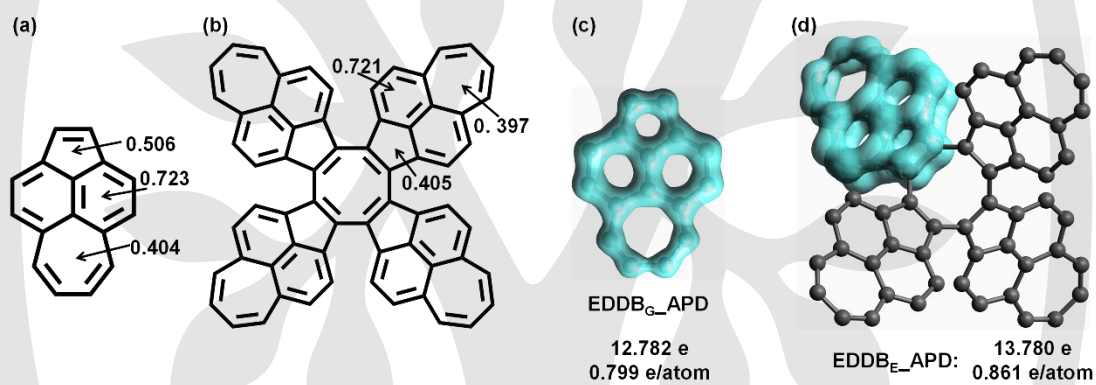


**Figure S6.** Calculated HOMA values of (a) APD and (b) APD moiety in COT-APD. The EDDB results of (c) APD and (d) APD moiety in COT-APD. The EDDB<sub>G</sub> is the delocalized electrons for the entire molecular system (excluding hydrogens), and the EDDB<sub>E</sub> is for the molecular fragment (including non-local effects).

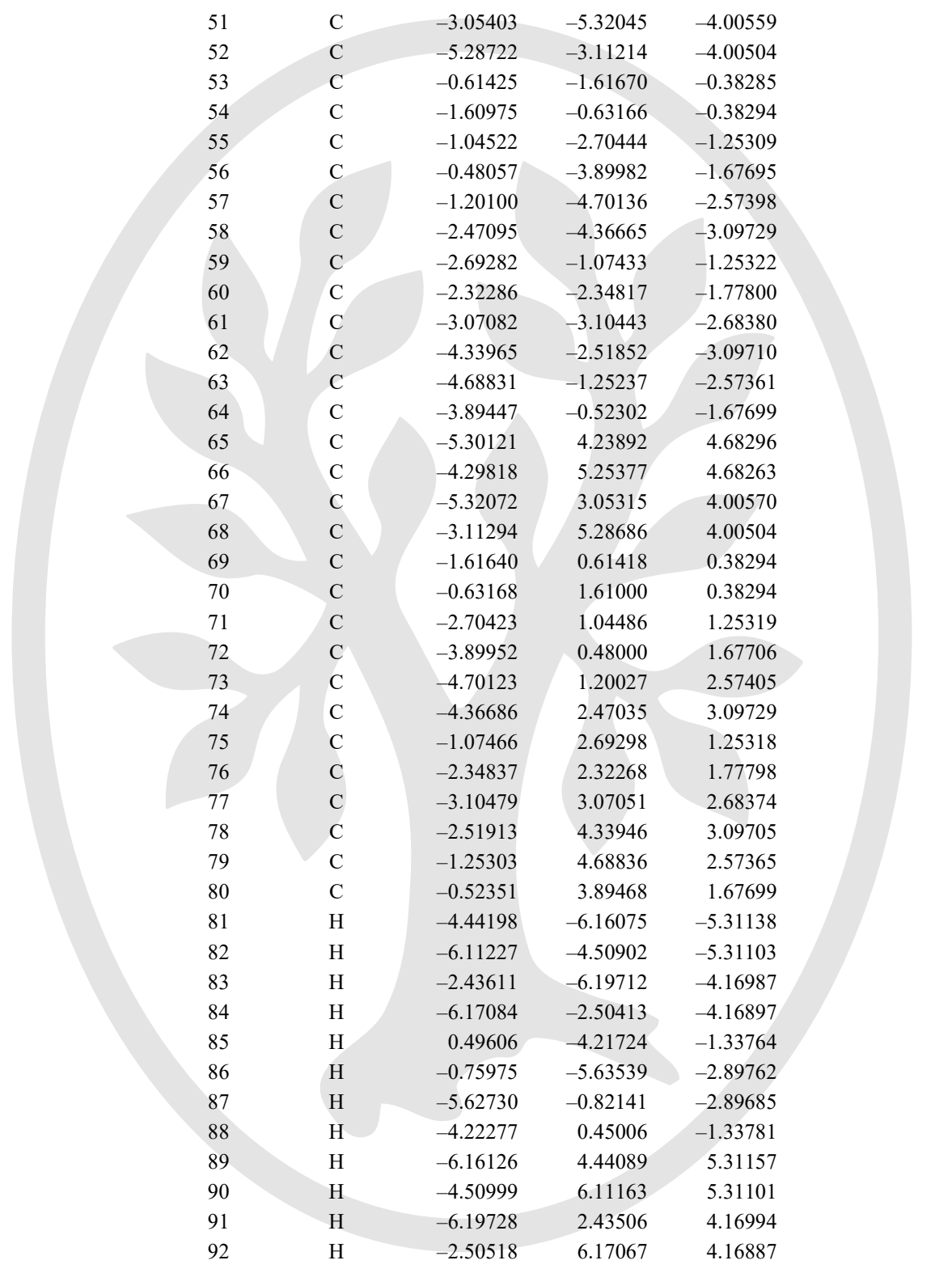
**Table S2.** Summary of the major excitations (oscillator strength > 0.05) of COT-APD obtained by the TD-DFT calculation.

Excited States	Energy (eV)	Wavelength (nm)	Oscillator Strength	Major Contributions
S1	1.9752	627.71	0.0000	HOMO→LUMO(99%)
S2	2.2252	557.19	0.0992	HOMO-1→LUMO(81%) HOMO→LUMO+1(13%)
S3	2.2253	557.14	0.0992	HOMO-2→LUMO (81%) HOMO→LUMO+2(13%)
S4	2.3118	536.31	0.0891	HOMO-3→LUMO (83%) HOMO→LUMO+3(13%)
S6	2.4716	501.64	0.2440	HOMO-2→LUMO+4 (2%) HOMO-1→LUMO (12%) HOMO→LUMO+1 (80%) HOMO→LUMO+6 (4%)
S7	2.4717	501.62	0.2436	HOMO-2→LUMO (12%) HOMO-1→LUMO+4 (2%) HOMO→LUMO+2 (80%) HOMO→LUMO+7 (4%)
S22	2.9115	425.84	0.0670	HOMO-4→LUMO+1 (17%) HOMO-2→LUMO+3 (11%) HOMO-1→LUMO+4 (22%) HOMO-1→LUMO+5 (4%) HOMO→LUMO+2 (3%) HOMO→LUMO+7 (36%)
S23	2.9116	425.83	0.0671	HOMO-4→LUMO+2 (17%) HOMO-2→LUMO+4 (22%) HOMO-2→LUMO+5 (4%) HOMO-1→LUMO+3 (11%) HOMO→LUMO+1 (3%) HOMO→LUMO+6 (36%)
S24	2.9462	420.82	0.7990	HOMO-4→LUMO+4 (5%) HOMO-3→LUMO (7%) HOMO-2→LUMO+2 (19%) HOMO-1→LUMO+1 (19%) HOMO→LUMO+3 (47%)
S30	3.0698	403.88	0.1488	HOMO-5→LUMO (57%) HOMO-4→LUMO+2 (22%) HOMO-3→LUMO+1 (2%) HOMO-2→LUMO+5 (9%) HOMO→LUMO+6 (4%)

## Cartesian coordinate of COT-APD

$E(\text{B3LYP}/6\text{-}31\text{G}^*) = -2458.090471$  Hartree

Tag	Symbol	X	Y	Z
1	C	4.29831	-5.25376	4.68256
2	C	5.30134	-4.23892	4.68285
3	C	3.11303	-5.28684	4.00503
4	C	5.32083	-3.05315	4.00559
5	C	0.63169	-1.61004	0.38293
6	C	1.61641	-0.61423	0.38288
7	C	1.07468	-2.69299	1.25319
8	C	0.52354	-3.89468	1.67704
9	C	1.25307	-4.68835	2.57369
10	C	2.51916	-4.33942	3.09710
11	C	2.70426	-1.04488	1.25313
12	C	2.34838	-2.32266	1.77799
13	C	3.10480	-3.07046	2.68379
14	C	4.36690	-2.47032	3.09727
15	C	4.70132	-1.20031	2.57390
16	C	3.89960	-0.48005	1.67691
17	C	5.25427	4.29742	-4.68269
18	C	4.23968	5.30071	-4.68289
19	C	5.28711	3.11215	-4.00514
20	C	3.05394	5.32047	-4.00559
21	C	1.60973	0.63162	-0.38301
22	C	0.61423	1.61666	-0.38287
23	C	2.69279	1.07431	-1.25328
24	C	3.89439	0.52297	-1.67714
25	C	4.68822	1.25234	-2.57376
26	C	4.33962	2.51856	-3.09711
27	C	1.04519	2.70443	-1.25309
28	C	2.32284	2.34819	-1.77799
29	C	3.07081	3.10448	-2.68375
30	C	2.47092	4.36670	-3.09724
31	C	1.20095	4.70137	-2.57393
32	C	0.48055	3.89982	-1.67690
33	H	4.51013	-6.11162	5.31094
34	H	6.16140	-4.44088	5.31145
35	H	2.50523	-6.17061	4.16896
36	H	6.19735	-2.43502	4.16986
37	H	-0.44948	-4.22318	1.33785
38	H	0.82230	-5.62741	2.89699
39	H	5.63527	-0.75886	2.89750
40	H	4.21682	0.49665	1.33762
41	H	6.11213	4.50903	-5.31114
42	H	4.44185	6.16077	-5.31144
43	H	6.17077	2.50418	-4.16904
44	H	2.43606	6.19718	-4.16977
45	H	4.22266	-0.45015	-1.33803
46	H	5.62717	0.82135	-2.89708



47	H	0.75969	5.63539	-2.89757
48	H	-0.49611	4.21722	-1.33762
49	C	-4.23980	-5.30070	-4.68283
50	C	-5.25440	-4.29741	-4.68259
51	C	-3.05403	-5.32045	-4.00559
52	C	-5.28722	-3.11214	-4.00504
53	C	-0.61425	-1.61670	-0.38285
54	C	-1.60975	-0.63166	-0.38294
55	C	-1.04522	-2.70444	-1.25309
56	C	-0.48057	-3.89982	-1.67695
57	C	-1.20100	-4.70136	-2.57398
58	C	-2.47095	-4.36665	-3.09729
59	C	-2.69282	-1.07433	-1.25322
60	C	-2.32286	-2.34817	-1.77800
61	C	-3.07082	-3.10443	-2.68380
62	C	-4.33965	-2.51852	-3.09710
63	C	-4.68831	-1.25237	-2.57361
64	C	-3.89447	-0.52302	-1.67699
65	C	-5.30121	4.23892	4.68296
66	C	-4.29818	5.25377	4.68263
67	C	-5.32072	3.05315	4.00570
68	C	-3.11294	5.28686	4.00504
69	C	-1.61640	0.61418	0.38294
70	C	-0.63168	1.61000	0.38294
71	C	-2.70423	1.04486	1.25319
72	C	-3.89952	0.48000	1.67706
73	C	-4.70123	1.20027	2.57405
74	C	-4.36686	2.47035	3.09729
75	C	-1.07466	2.69298	1.25318
76	C	-2.34837	2.32268	1.77798
77	C	-3.10479	3.07051	2.68374
78	C	-2.51913	4.33946	3.09705
79	C	-1.25303	4.68836	2.57365
80	C	-0.52351	3.89468	1.67699
81	H	-4.44198	-6.16075	-5.31138
82	H	-6.11227	-4.50902	-5.31103
83	H	-2.43611	-6.19712	-4.16987
84	H	-6.17084	-2.50413	-4.16897
85	H	0.49606	-4.21724	-1.33764
86	H	-0.75975	-5.63539	-2.89762
87	H	-5.62730	-0.82141	-2.89685
88	H	-4.22277	0.45006	-1.33781
89	H	-6.16126	4.44089	5.31157
90	H	-4.50999	6.11163	5.31101
91	H	-6.19728	2.43506	4.16994
92	H	-2.50518	6.17067	4.16887
93	H	-4.21671	-0.49673	1.33784
94	H	-5.63513	0.75879	2.89774
95	H	-0.82223	5.62742	2.89694
96	H	0.44952	4.22315	1.33782



## 5. References

- (1) Fu, L.; Liu, P.; Xue, R.; Tang, X.-Y.; Cao, J.; Yao, Z. F.; Liu, Y.; Yan, S.; Wang, X.-Y. *Angew. Chem. Int. Ed.* **2023**, *62*, e202306509.
- (2) Liu, P.; Chen, X.-Y.; Cao, J.; Ruppenthal, L.; Gottfried, J. M.; Müllen, K.; Wang, X.-Y. *J. Am. Chem. Soc.* **2021**, *143*, 5314.
- (3) Sumy, D. P.; Dodge, N. J.; Harrison, C. M.; Finke, A. D.; Whalley, A. C. *Chem. Eur. J.* **2016**, *22*, 4709.
- (4) Kumar, R.; Chmielewski, P. J.; Lis, T.; Volkmer, D.; Stępień, M. *Angew. Chem. Int. Ed.* **2022**, *61*, e202207486.
- (5) Urieta-Mora, J.; Krug, M.; Alex, W.; Perles, J.; Fernández, I.; Molina-Ontoria, A.; Guldi, D. M.; Martín, N. *J. Am. Chem. Soc.* **2020**, *142*, 4162.
- (6) Gaussian 09, Revision D.01, Frisch, M. J.; Trucks, G. W.; Schlegel, H. B.; Scuseria, G. E.; Robb, M. A.; Cheeseman, J. R.; Scalmani, G.; Barone, V.; Mennucci, B.; Petersson, G. A.; Nakatsuji, H.; Caricato, M.; Li, X.; Hratchian, H. P.; Izmaylov, A. F.; Bloino, J.; Zheng, G.; Sonnenberg, J. L.; Hada, M.; Ehara, M.; Toyota, K.; Fukuda, R.; Hasegawa, J.; Ishida, M.; Nakajima, T.; Honda, Y.; Kitao, O.; Nakai, H.; Vreven, T.; Montgomery, Jr., J. A.; Peralta, J. E.; Ogliaro, F.; Bearpark, M.; Heyd, J. J.; Brothers, E.; Kudin, K. N.; Staroverov, V. N.; Kobayashi, R.; Normand, J.; Raghavachari, K.; Rendell, A.; Burant, J. C.; Iyengar, S. S.; Tomasi, J.; Cossi, M.; Rega, N.; Millam, N. J.; Klene, M.; Knox, J. E.; Cross, J. B.; Bakken, V.; Adamo, C.; Jaramillo, J.; Gomperts, R.; Stratmann, R. E.; Yazyev, O.; Austin, A. J.; Cammi, R.; Pomelli, C.; Ochterski, J. W.; Martin, R. L.; Morokuma, K.; Zakrzewski, V. G.; Voth, G. A.; Salvador, P.; Dannenberg, J. J.; Dapprich, S.; Daniels, A. D.; Farkas, Ö.; Foresman, J. B.; Ortiz, J. V.; Cioslowski, J.; Fox, D. J. Gaussian, Inc., Wallingford CT, 2013.
- (7) Geuenich, D.; Hess, K.; Köhler, F.; Herges, R. *Chem. Rev.* **2005**, *105*, 3758.
- (8) Chen, Z.; Wannere, C. S.; Corminboeuf, C.; Puchta, R.; Schleyer, P. V. R. *Chem. Rev.* **2005**, *105*, 3842.
- (9) Krygowski, T. M.; Cyrańska, M. K. *Phys. Chem. Chem. Phys.* **2004**, *6*, 249.
- (10)(a) Klod, S.; Koch, A.; Kleinpeter, E. *J. Chem. Soc., Perkin Trans.* **2002**, 1506. (b) Lu, T.; Chen, F. *J. Comput. Chem.* **2012**, *33*, 580.
- (11) Szczepanik, D. W.; Andrzejak, M.; Dyduch, K.; Żak, E.; Makowski, M.; Mazur, G.; Mrozek, J. *Phys Chem Chem Phys*, **2014**, *16*, 20514.

## 6. NMR spectra

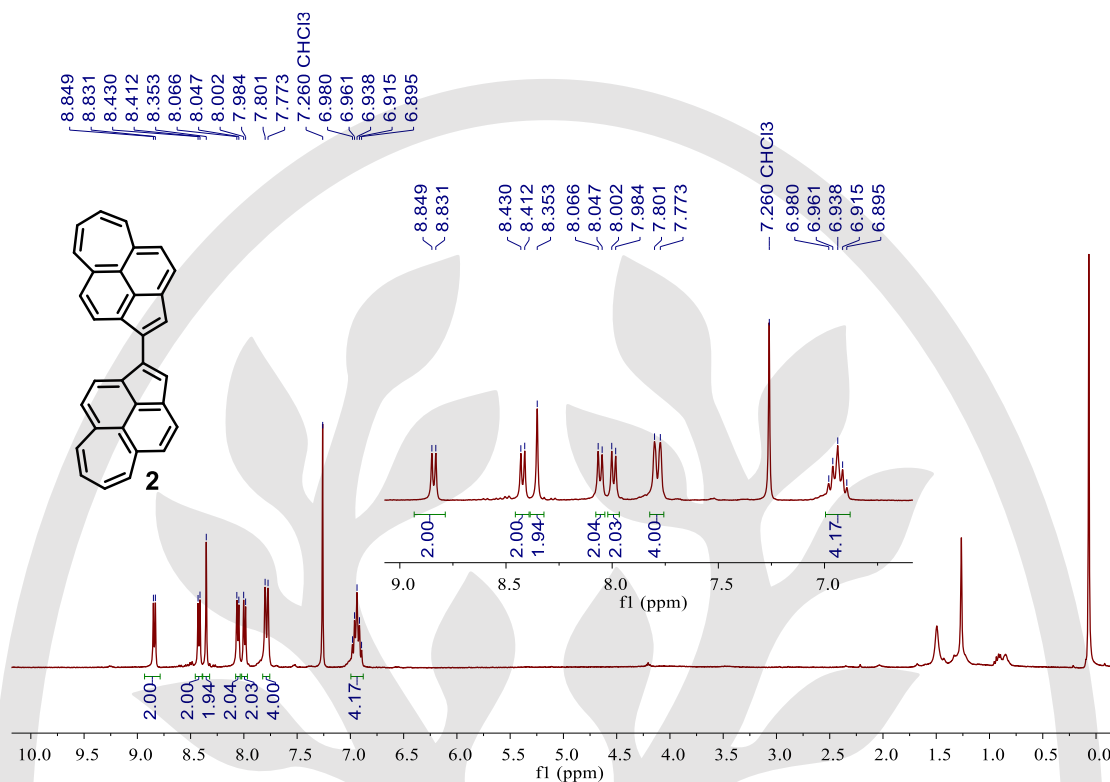


**Figure S7.** <sup>1</sup>H NMR spectrum of compound 2 (400 MHz, CDCl<sub>3</sub>, 298 K).

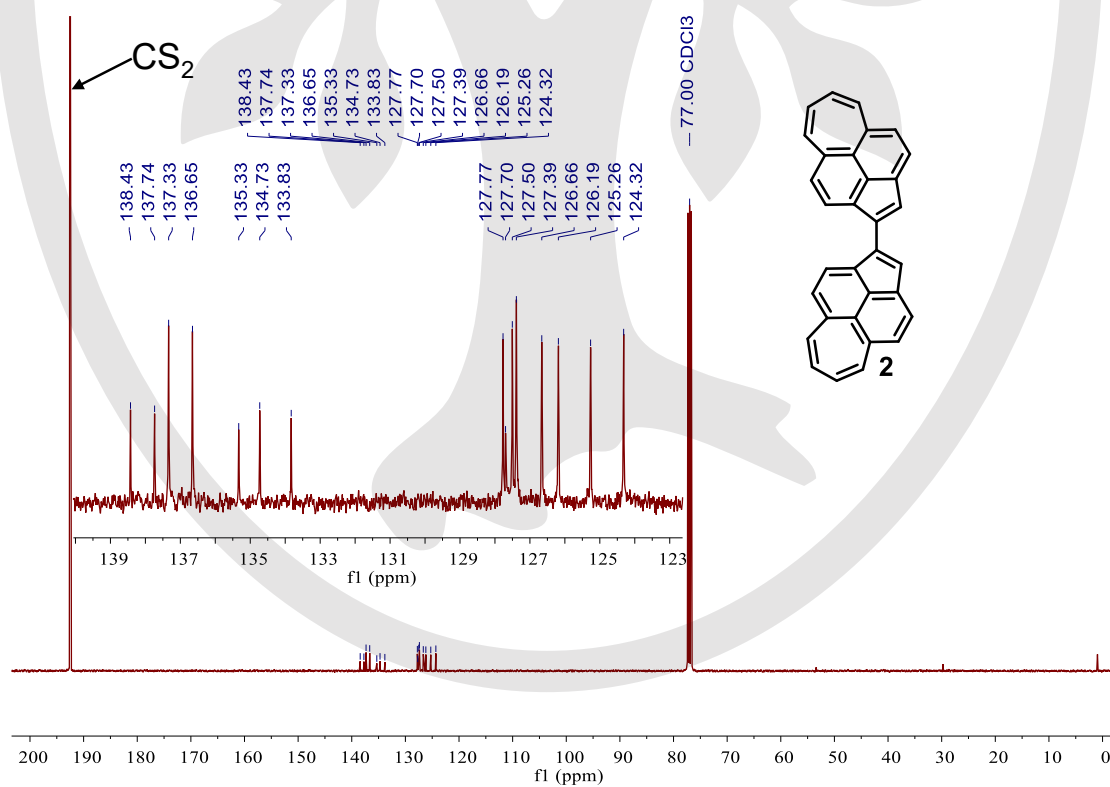


**Figure S8.** <sup>13</sup>C NMR spectrum of compound 2 (101 MHz, CS<sub>2</sub>/CDCl<sub>3</sub>, 298 K).

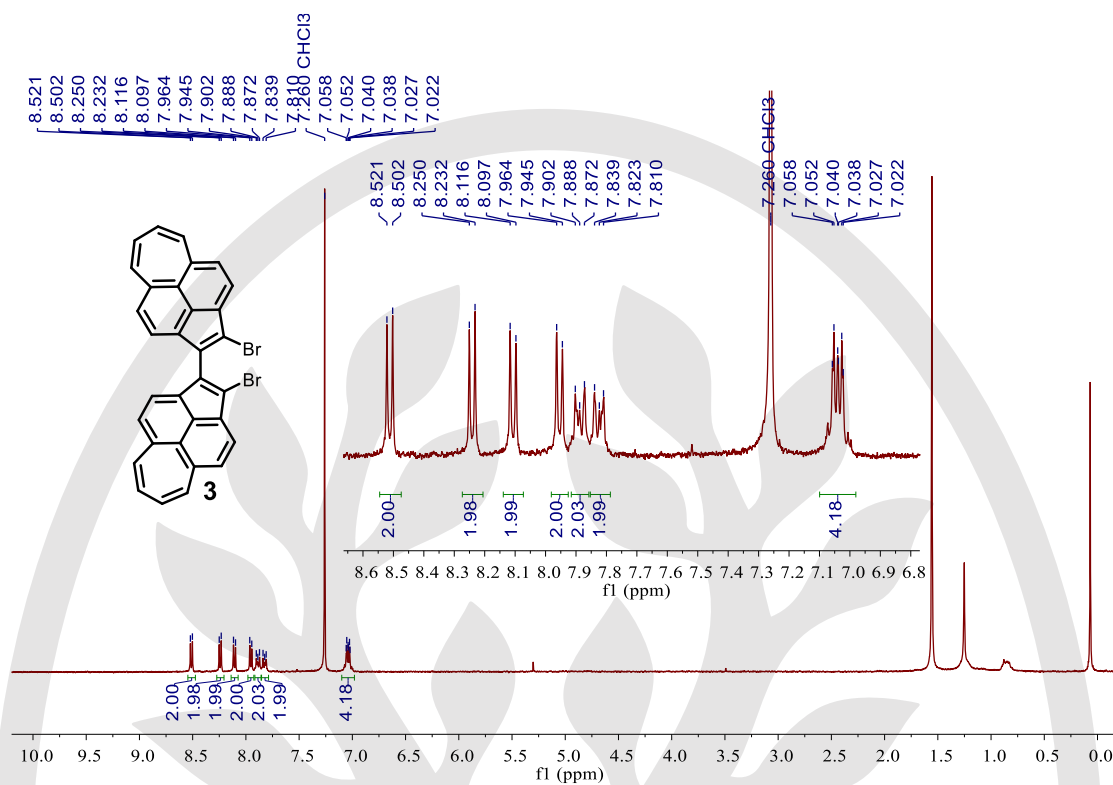


**Figure S9.**  $^1\text{H}$  NMR spectrum of compound **3** (400 MHz,  $\text{CDCl}_3$ , 298 K).

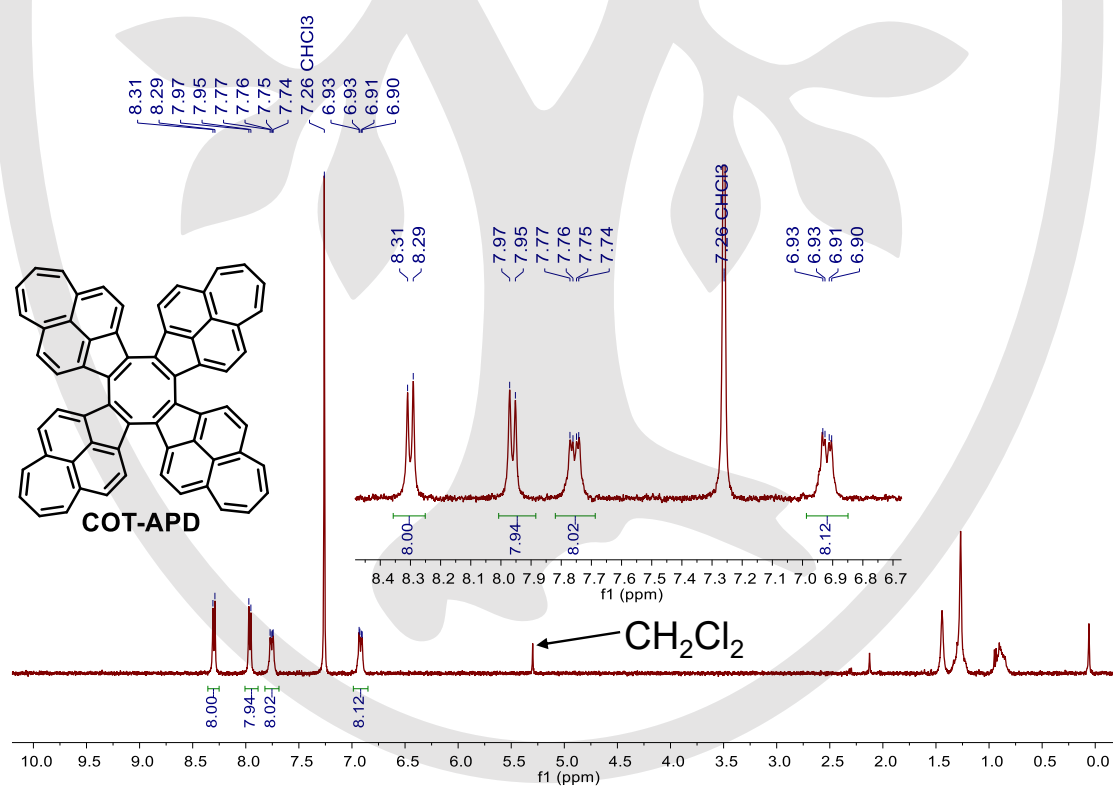


**Figure S10.**  $^1\text{H}$  NMR spectrum of **COT-APD** (400 MHz,  $\text{CS}_2/\text{CDCl}_3$ , 298 K).

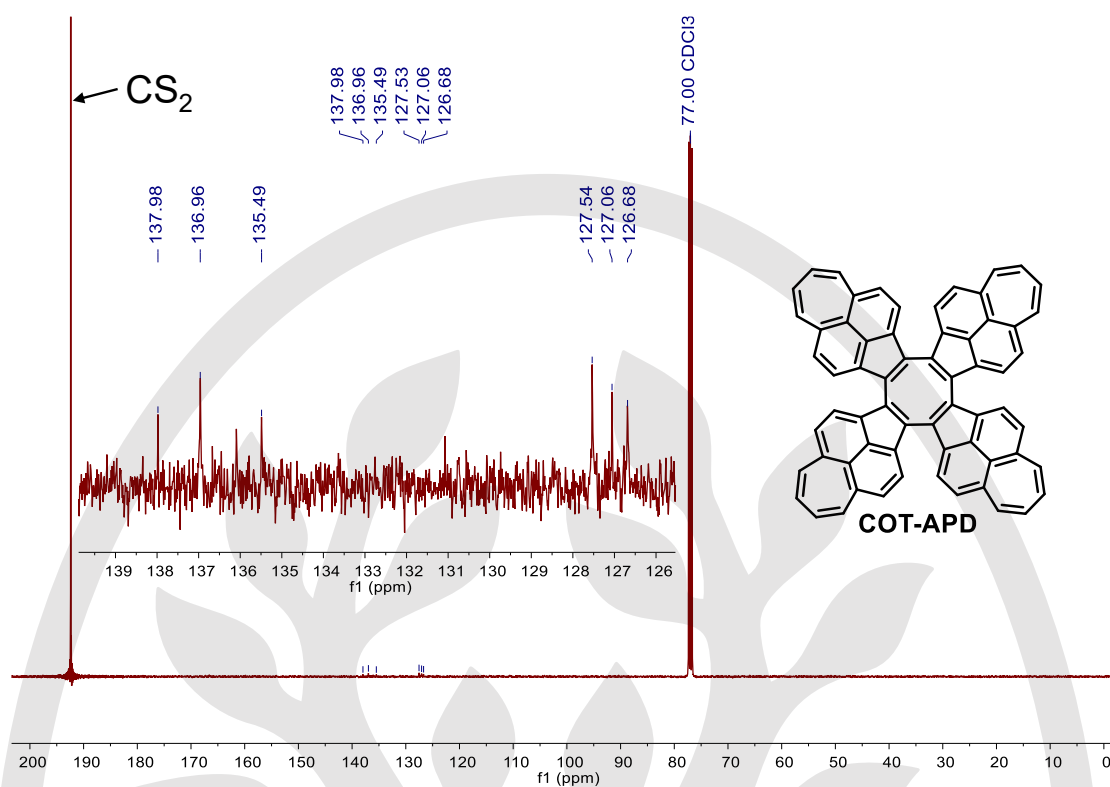


**Figure S11.** <sup>13</sup>C NMR spectrum of COT-APD (101 MHz, CS<sub>2</sub>/CDCl<sub>3</sub>, 298 K, number of scans: 18705).

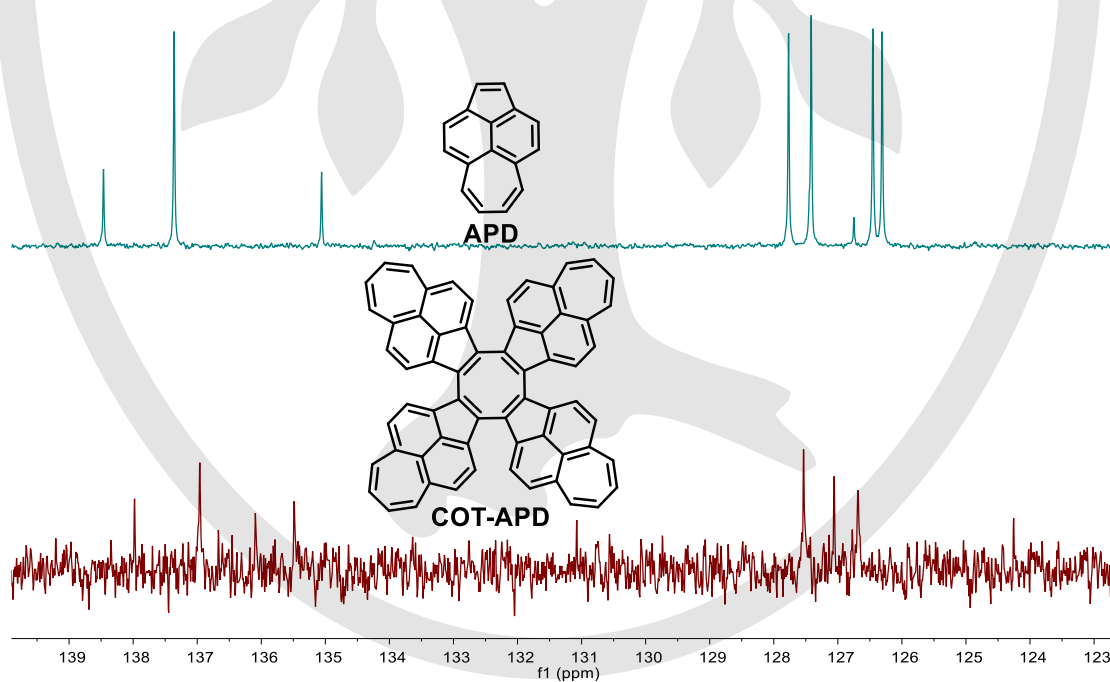


**Figure S12.** Comparison of <sup>13</sup>C NMR spectra of APD and COT-APD (101 MHz, CS<sub>2</sub>/CDCl<sub>3</sub>, 298 K).